COMPDYN 2011
III ECCOMAS Thematic Conference on
Computational Methods in Structural Dynamics and Earthquake Engineering
M. Papadrakakis, M. Fragiadakis, V. Plevris (eds.)
Corfu, Greece, 25–28 May 2011

HIGH CONTINUITY SECOND-ORDER HOMOGENIZATION OF IN-PLANE LOADED PERIODIC MASONRY

A. Bacigalupo[1] **and L. Gambarotta**[2]

[1] Department of Civil, Environmental and Architectural Engineering
via Montallegro, 1 – 16145 Genova, Italy
e-mail: andrea.bacigalupo@unige.it

[2] Department of Civil, Environmental and Architectural Engineering
via Montallegro, 1 – 16145 Genova, Italy
gambarotta@dicat.unige.it

Keywords: Masonry, Second-order homogenization, Boundary layer effects, Dispersive waves, Material characteristic length.

Abstract. *In this paper the second-order homogenization of periodic masonry based on a computational analysis of the unit cell representative of the masonry wall is derived. The multi-scale approach is based on an appropriate representation of the micro-displacement field as the superposition of a local macroscopic displacement field, represented in a polynomial form related to the macro-displacement field, and an unknown micro-fluctuation field accounting for the effects of the heterogeneities. By this approach a continuous micro-displacement field is obtained, i.e. in each unit cell and across the interfaces between adjacent unit cells. The computational procedure is applied in two steps: the first one corresponds to the standard homogenization, while the second step is a second-order homogenization based on the results of the first step. Two numerical examples are presented concerning running bond and English bond masonry. For both the masonry patterns the overall elastic moduli of the second-order model and the corresponding characteristic lengths are obtained; the effects on the characteristic lengths of the stiffness mismatch between the brick phase and the mortar phase are considered. Moreover, the wave propagation in the homogenized medium is considered and dispersive waves are obtained. It is shown that remarkable differences in the phase and group velocities between the first-order and the second-order homogenized models are obtained for wavelengths shorter than ten times the average brick unit size.*

1 INTRODUCTION

The non-local homogenization of periodic masonry is a subject of some interest because in many cases the brick size is not negligible if compared with the structural size, the characteristic length of applied forces or, finally, the wavelength of waves propagating in the wall.

Cosserat constitutive models of periodic masonry have been proposed by several Authors [1-4] as result of homogenization procedures based on an idealization of the masonry as an assemblage of rigid blocks interacting through linear elastic interfaces represented as a Lagrangian system. To overcome the limits deriving from the assumption of rigid blocks Casolo [5] proposed a Cosserat homogenization based on a heuristic evaluation of the mean local rotation of the brick units. The Cosserat homogenization technique proposed by Forest and Sab [6] for continuously deformable heterogeneous media has been extended to periodic masonry by Bacigalupo and Gambarotta [7,8] and by Addessi *et al.* [9], the last contribution to include elasto-damage constitutive equations at the microscale. In Bacigalupo and Gambarotta [8] an evaluation of the reliability of Cosserat homogenization has been carried out by analysing a boundary shear layer problem concerning a masonry wall. The extension of this analysis to second-order homogenization has shown this last one to be more suitable with respect to the micropolar models (Cosserat and Couple-stresses models).

Although second-order homogenization techniques have been proposed through an extension of the classical asymptotic homogenization theory [10-13], they have not been applied in the past to the homogenization of periodic masonry because, as observed by Peerlings and Fleck [14], they result to be computationally burdensome.

The second-order computational procedure here considered is obtained by the analysis of the unit cell representative of the heterogeneous periodic material and is based on an enhanced representation of the micro-displacement field as the superposition of a local macroscopic displacement field, expressed in a polynomial form related to the macro-displacement field, and an unknown micro-fluctuation field accounting for the effects of the heterogeneities [15]. This assumption guarantees the resulting micro-fluctuation field to be continuous on the masonry domain, i.e. in each unit cell and across the interfaces between adjacent unit cells.

Running bond masonry and English bond masonry are analyzed through the second-order homogenization procedure here considered and the elastic moduli and the characteristic lengths of the equivalent continuous are obtained. Moreover, the wave propagation along the symmetry lines of the equivalent orthotropic continuum is analysed. Dispersive waves are obtained and the resulting phase and group velocity are evaluated at different wavelengths.

2 MULTI-SCALE IN-PLANE MODELLING OF PERIODIC MASONRY

Let us consider a masonry wall with periodic arrangement of the bricks in its own plane as shown in Figure 1.a. If only in-plane loads are envisaged and body forces are neglected, the masonry wall may be represented as a plane domain under the simplifying assumption of plane stress condition. The obtained heterogeneous model is analysed as a Cauchy continuum undergoing small strains and the phases are assumed to behave elastically. The position vector $\mathbf{x}$ of a material point is denoted by its components (x_1,x_2) with respect to the reference $(0,\mathbf{e}_1,\mathbf{e}_2)$. The periodic continuum is fully characterized by the unit cell $\mathcal{A}=[0,d_1]\times[0,d_2]$ shown in figure 1.b (width d_1 and height d_2), i.e. the smallest plane portion that contains all the essential information about the masonry pattern. This unit cell is spanned by the two independent orthogonal vectors $\mathbf{v}_1=d_1\mathbf{e}_1$, $\mathbf{v}_2=d_2\mathbf{e}_2$, so that the boundary C of the unit cell is made up of two pairs of opposite sides corresponding to each other by means of a translation

along $\mathbf{v}_1$ or $\mathbf{v}_2$. According to this representation, a variable is periodic in the unit cell $\mathcal{A}$, or $\mathcal{A}$-periodic, if it takes identical values at two points on the boundary of the unit cell whose difference is a vector of periodicity. In this sense, the elasticity tensor $\mathbb{C}^m(\mathbf{x})$ is $\mathcal{A}$-periodic, i.e. $\mathbb{C}^m(\mathbf{x}+\mathbf{v}_i)=\mathbb{C}^m(\mathbf{x})$, i=1,2.

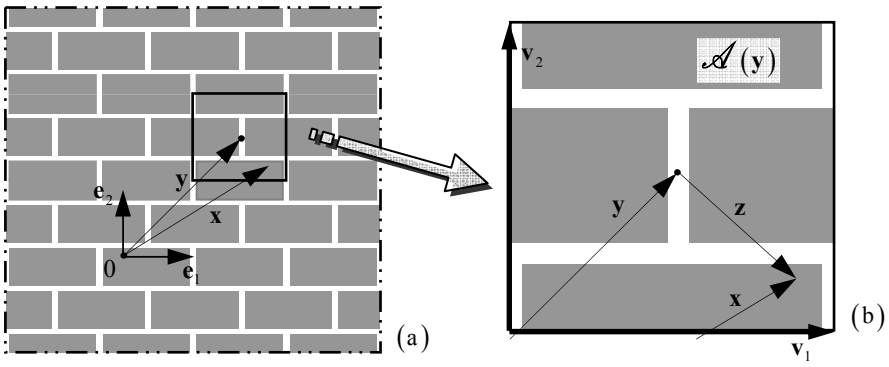

Fig. 1 (a) Periodic masonry; (b) Unit cell and periodicity vectors.

At the material point $\mathbf{x}$ of the heterogeneous elastic medium the micro-displacement $\mathbf{u}(\mathbf{x},t)$ is considered together with the corresponding micro-strain tensor $\boldsymbol{\varepsilon}(\mathbf{x},t)=sym\nabla_{\mathbf{x}}\mathbf{u}(\mathbf{x},t)$ and the micro-stress tensor $\boldsymbol{\sigma}(\mathbf{x},t)=\mathbb{C}^m(\mathbf{x})\boldsymbol{\varepsilon}(\mathbf{x},t)$ which has to satisfy the local equation of motion $div_{\mathbf{x}}\boldsymbol{\sigma}(\mathbf{x},t)=\rho\ddot{\mathbf{u}}(\mathbf{x},t)$. The resulting set of partial differential equations

$$div_{\mathbf{x}}\left(\mathbb{C}^m(\mathbf{x})\nabla_{\mathbf{x}}\mathbf{u}(\mathbf{x},t)\right)=\rho\ddot{\mathbf{u}}(\mathbf{x},t) \tag{1}$$

has to be solved in terms of the micro-displacement components on the whole masonry wall domain with a remarkable computational burden.

Being the solution of this fine-scale computational approach out of reach, it is convenient to replace the heterogeneous model of masonry wall by an equivalent homogeneous one so obtaining equations whose coefficients are not rapidly oscillating while their solutions are close to those of the original equations. In general, an equivalent standard (Cauchy) continuum is considered, but in cases for which the unit cell size is non vanishing if compared to the wall size or to the wavelength it is convenient to introduce an equivalent second-order continuum model [16]. This continuum model is defined at the macroscale where the slow varying macroscopic position vector $\mathbf{y}$ is considered and the displacement field $\mathbf{U}(\mathbf{y},t)$ is defined (with component U_i in the assumed reference). The displacement gradient is denoted by $\mathbf{H}(\mathbf{y},t)=\nabla_{\mathbf{y}}\mathbf{U}(\mathbf{y},t)$ and, according to Germain [17], the strain field in the second gradient continuum is represented by the symmetric first-order strain tensor and by the second-order strain tensor, respectively,

$$\mathbf{E}(\mathbf{y},t)=sym\nabla_{\mathbf{y}}\mathbf{U}(\mathbf{y},t),\qquad \boldsymbol{\kappa}(\mathbf{y},t)=\nabla_{\mathbf{y}}\otimes\nabla_{\mathbf{y}}\mathbf{U}(\mathbf{y},t), \tag{2}$$

the latter being a third-order tensor having components $\kappa_{ijk}=\kappa_{ikj}$ symmetric with respect to j and k.

The stress field is described by the symmetric first-order stress tensor $\boldsymbol{\Sigma}(\mathbf{y},t)$ ($\Sigma_{ij}=\Sigma_{ji}$) and by second-order stress tensor $\boldsymbol{\mu}(\mathbf{y},t)$ (third-order tensor having components $\mu_{ijk}=\mu_{ikj}$ symmetric with respect to j and k). From these stress tensors the real stress at the macro-scale is defined as $\mathbf{T}(\mathbf{y},t)=\boldsymbol{\Sigma}(\mathbf{y},t)-Div_{\mathrm{y}}\boldsymbol{\mu}(\mathbf{y},t)$ so that, in general, $\mathbf{T}(\mathbf{y},t)$ is not symmetric. In case of vanishing body forces, the equation of motion is expressed according to Mindlin [16] in the form

$$Div_{\mathrm{y}}\left(\boldsymbol{\Sigma}(\mathbf{y},t)-Div_{\mathrm{y}}\boldsymbol{\mu}(\mathbf{y},t)\right)=\rho_M\left[\ddot{\mathbf{U}}(\mathbf{y},t)-\left(\nabla_{\mathrm{y}}\otimes\nabla_{\mathrm{y}}\ddot{\mathbf{U}}(\mathbf{y},t)\right)\mathbf{J}\right], \tag{3}$$

being the inertia properties defined by the mass density at the macro-scale ρ_M and the inertia tensor $\mathbf{J}=\int_{\mathcal{A}}\rho\mathbf{y}\otimes\mathbf{y}da\Big/\int_{\mathcal{A}}\rho da$, where ρ is the mass density at the micro-scale. The first-order and second-order stress tensors are energetically conjugate to the corresponding strain tensors by the virtual power theorem; therefore, the constitutive equations in case of linear elasticity take the form

$$\boldsymbol{\Sigma}=\mathbb{C}\mathbf{E}+\mathbb{Y}\boldsymbol{\kappa},\qquad \boldsymbol{\mu}=\mathbb{Y}\mathbf{E}+\mathbb{S}\boldsymbol{\kappa}, \tag{4}$$

$\mathbb{C}$ being the (standard) fourth-order elasticity tensor, $\mathbb{S}$ the sixth order tensor related to second-order stress and strain tensors and $\mathbb{Y}$ a fifth order tensor taking into account the coupling between the first and second-order stress and strain tensors. The equation of motion of the second order continuum is obtained for centro-symmetric unit cells, namely with vanishing tensor $\mathbb{Y}$, from the field equations (2), (3) and (4) and takes the form

$$Div_{\mathrm{y}}\left(\mathbb{C}\nabla_{\mathrm{y}}\mathbf{U}(\mathbf{y},t)-Div_{\mathrm{y}}\mathbb{S}\nabla_{\mathrm{y}}\otimes\nabla_{\mathrm{y}}\mathbf{U}(\mathbf{y},t)\right)=\rho_M\left[\ddot{\mathbf{U}}(\mathbf{y},t)-\left(\nabla_{\mathrm{y}}\otimes\nabla_{\mathrm{y}}\ddot{\mathbf{U}}(\mathbf{y},t)\right)\mathbf{J}\right], \tag{5}$$

or in components

$$C_{ijhk}U_{h,kj}-S_{ijkrpq}U_{r,pqjk}=\rho_M\left(\ddot{U}_i-J_{kk}\ddot{U}_{i,kk}\right),\qquad i=1,2,3. \tag{6}$$

In order to replace the first-order heterogeneous model, where the micro-fields are defined, with the second-order homogeneous equivalent medium, the variables defined at the corresponding scales have to be properly coupled by means of transition strategies for the strains and strains gradients from the macroscale to the discribed microstructure. In the following, a kinematic multi-scale model proposed by the Authors [15] is considered.

3 SECOND ORDER HOMOGENIZATION OF PERIODIC MATERIALS

In order to couple the kinematics of the classical continuum at the micro-scale to the kinematics of the second-order continuum at the macro-scale, the micro-displacement field in the unit cell is represented in the form $\mathbf{u}(\mathbf{x},t)=\mathbf{u}(\mathbf{y},\mathbf{z},t)$. Here, $\mathbf{y}$ denotes the position vector of the unit cell in which $\mathbf{x}$ is located and vector $\mathbf{z}=\mathbf{x}-\mathbf{y}$ its relative position. This representation highlights the dependence of the displacement field on both the unit cell position $\mathbf{y}$, called the macro-position, and the local position $\mathbf{z}$ at a point of interest. The effective micro-displacement field $\mathbf{u}(\mathbf{y},\mathbf{z},t)$ is approximated by the vector field

$$\mathbf{u}(\mathbf{y},\mathbf{z},t)\approx\mathbf{u}^{\alpha}(\mathbf{y},\mathbf{z},t)=\mathbf{U}(\mathbf{y},t)+\mathbf{H}(\mathbf{y},t)\mathbf{z}+\frac{1}{2}\boldsymbol{\kappa}(\mathbf{y},t):(\mathbf{z}\otimes\mathbf{z})+\tilde{\mathbf{u}}(\mathbf{y},\mathbf{z},t), \tag{7}$$

superposition of a polynomial function depending on both the macro-displacement and the macro-strain fields and a complementary displacement field $\tilde{\mathbf{u}}(\mathbf{y},\mathbf{z},t)$ that represents the microstructural displacement fluctuation field at the microscale due to the inhomogeneities. To obtain continuous micro-displacement fields across the unit cell interfaces, the complementary displacement field is assumed according to [15], in the form

$$\tilde{\mathbf{u}}(\mathbf{y},\mathbf{z},t)=\mathbf{r}^1(\mathbf{y},\mathbf{z},t)+\mathbf{r}^2(\mathbf{y},\mathbf{z},t), \tag{8}$$

each of them having the following representation in components

$$r_i^1(\mathbf{y},\mathbf{z},t)=\theta_{ikl}^1(\mathbf{z})\left[H_{kl}(\mathbf{y},t)+\kappa_{klp}(\mathbf{y},t)z_p\right],\quad r_i^2(\mathbf{y},\mathbf{z},t)=\theta_{iklp}^2(\mathbf{z})\kappa_{klp}(\mathbf{y},t), \tag{9}$$

where the functions $\theta_{ikl}^1(\mathbf{z})$ and $\theta_{iklp}^2(\mathbf{z})$ have to satisfy the condition of $\mathcal{A}$-periodicity, namely $\theta_{ikl}^1(\mathbf{z}_0^i+\mathbf{v}_i)=\theta_{ikl}^1(\mathbf{z}_0^i)$ and $\theta_{iklp}^2(\mathbf{z}_0^i+\mathbf{v}_i)=\theta_{iklp}^2(\mathbf{z}_0^i)$, $\forall\mathbf{z}_0^i\in C_i$, i=1,2 .

The representation of the micro-displacement fluctuation field (9) in the unit cell $\mathcal{A}(\mathbf{y})$ is the key point on which the following two-step computational homogenization is based. The first step is the standard first-order homogenization in which the unknown functions $\theta_{ikl}^1(\mathbf{z})$ have to be evaluated. Here the function $\theta_{ikl}^1(\mathbf{z})$ represents the fluctuation displacement along direction $\mathbf{e}_i$ associated to the homogeneous component $H_{kl}=1$ of the macro-displacement gradient; it is obtained by the computational analysis of the unit cell $\mathcal{A}(\mathbf{y})$ with prescribed classic periodic boundary conditions on the micro-displacement field

$$\mathbf{u}^I(\mathbf{z}_b+\mathbf{v}_i)-\mathbf{u}^I(\mathbf{z}_b)=\mathbf{H}\mathbf{v}_i,\qquad \forall\mathbf{z}_b\in C_i,\quad i=1,2, \tag{10}$$

where $\mathbf{z}_b$ is the local position vector at a point on the boundary C_i, $i=1,2$ (see figure 2.b). Once the micro-displacement $\mathbf{u}^I(\mathbf{z})$ in the unit cell $\mathcal{A}(\mathbf{y})$ is obtained for $H_{kl}=1$ prescribed, the 2^3 unknown functions $\theta_{ikl}^1(\mathbf{z})$ are evaluated $\theta_{ijk}^1(\mathbf{z})=u_{ijk}^I(\mathbf{z})-\delta_{ij}z_k$. Following this procedure for all the components of tensor $\mathbf{H}$ the overall (Cauchy) elasticity tensor $\mathbb{C}$ is evaluated through an application of the Hill-Mandel condition.

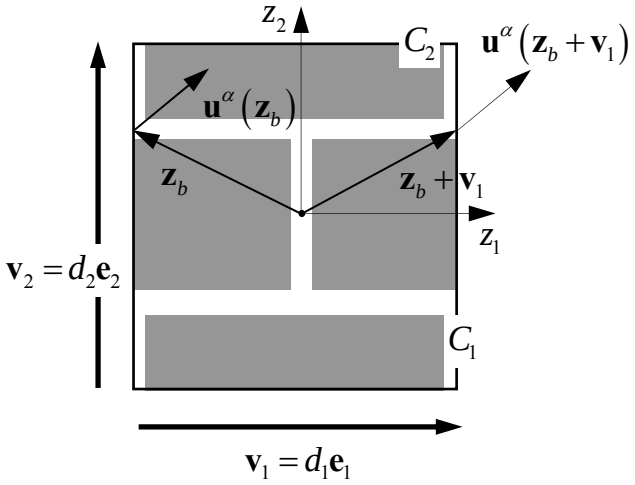

Fig. 2 Displacement vectors of points at the boundary of the unit cell.

The second step is carried out by considering a homogeneous second-order strain field and vanishing macro-strain $\mathbf{E}=\mathbf{0}$. The 2^4 unknown functions $\theta^2_{ijkl}(\mathbf{z})$ are obtained by analysing the unit cell $\mathscr{A}(\mathbf{y})$ with prescribed boundary conditions on the micro-displacement field derived from the $\mathscr{A}$-periodicity condition (9.2). For an arbitrary prescribed homogeneous second-order strain tensor $\boldsymbol{\kappa}$, the micro-displacement $\mathbf{u}^{II}(\mathbf{z})$ is written at corresponding points on the boundary $\mathbf{z}_b$ and $\mathbf{z}_b+\mathbf{v}_i$ (see figure 2) according to representation (7), (8), (9) and including the condition of $\mathscr{A}$-periodicity on the functions $\theta^2_{ijkl}(\mathbf{z})$

$$\mathbf{u}^{II}(\mathbf{z}_b+\mathbf{v}_i)-\mathbf{u}^{II}(\mathbf{z}_b)=\mathbf{u}^{*}(\mathbf{z}_b+\mathbf{v}_i)-\mathbf{u}^{*}(\mathbf{z}_b)+\boldsymbol{\Theta}^1(\mathbf{z}_b):\boldsymbol{\kappa}\mathbf{v}_i,\qquad \mathbf{z}_b\in C_i,\quad i=1,2, \tag{11}$$

$\boldsymbol{\Theta}^1$ being the third order tensor having components $\theta^1_{ikl}(\mathbf{z})$.

The boundary conditions referred to the vertical side C_1 and horizontal side C_2 are written in components in the following form, respectively:

$$\begin{aligned}
&u_i^{II}(z_1^+)-u_i^{II}(z_1^-)=u_i^{*}(z_1^+)-u_i^{*}(z_1^-)+\theta^{1+}_{i11}d_1\kappa_{111}+\theta^{1+}_{i12}d_1\kappa_{112}+\theta^{1+}_{i21}d_1\kappa_{211}+\theta^{1+}_{i22}d_1\kappa_{221},\\
&u_i^{II}(z_2^+)-u_i^{II}(z_2^-)=u_i^{*}(z_2^+)-u_i^{*}(z_2^-)+\theta^{1+}_{i11}d_2\kappa_{112}+\theta^{1+}_{i12}d_2\kappa_{122}+\theta^{1+}_{i21}d_2\kappa_{212}+\theta^{1+}_{i22}d_2\kappa_{222},
\end{aligned} \tag{12}$$

where the notation $z_i^{\pm}=\pm d_i/2$, $i=1,2$ and $\theta^{1+}_{hkl}=\theta^1_{hkl}(z_i^+)$ is assumed.

The corresponding micro-displacement field $\mathbf{u}^{II}(\mathbf{z})$ is obtained by a FE analysis of the unit cell under the assumption $\mathbf{E}=\mathbf{0}$ and $\boldsymbol{\kappa}$ homogeneous in the unit cell. Each displacement functions $\theta^2_{iklp}(\mathbf{z})$ is obtained from the displacement field $u^{II}_{iklp}(\mathbf{z})$ resulting by the FE analysis of the unit cell with prescribed non-zero component $\kappa_{klp}=1$, as follows

$$\theta^2_{iklp}(\mathbf{z})=u^{II}_{iklp}(\mathbf{z})-\frac{1}{2}\left(\delta_{ik}z_lz_p+\theta^1_{ikl}(\mathbf{z})z_p+\theta^1_{ikp}(\mathbf{z})z_l\right), \tag{13}$$

being the fluctuation $\theta^1_{ijk}(\mathbf{z})$ known from the first-order homogenization.

The elastic moduli of the second-order continuum are evaluated in the unit cell with reference to the macro-strain vectors $\underline{E}=\{H_{11}\quad H_{22}\quad H_{12}+H_{21}\}^{\mathrm{T}}$ and $\underline{\kappa}=\{\kappa_{111}\quad\kappa_{222}\quad\kappa_{122}\quad\kappa_{211}\quad\kappa_{121}\quad\kappa_{212}\quad\kappa_{112}\quad\kappa_{221}\}^{\mathrm{T}}$. The Hill-Mandel macro-homogeneity condition is applied $\mathscr{E}^{\circ}_M=\mathscr{E}^{\circ}_m$, where $\mathscr{E}^{\circ}_M$ is the macro-strain energy at a point $\mathbf{y}$ of the homogenized continuum written in the following quadratic form

$$\mathscr{E}^{\circ}_M(\underline{E},\underline{\kappa})=\frac{1}{2}\left\{\underline{E}^{\mathrm{T}}\quad\underline{\kappa}^{\mathrm{T}}\right\}\begin{bmatrix}\underline{\underline{C}} & \underline{\underline{Y}}\\ \underline{\underline{Y}}^{\mathrm{T}} & \underline{\underline{S}}\end{bmatrix}\begin{Bmatrix}\underline{E}\\ \underline{\kappa}\end{Bmatrix}. \tag{14}$$

In equation (14) $\underline{\underline{C}}$, $\underline{\underline{Y}}$ and $\underline{\underline{S}}$ are the sub-matrices of the second-order elastic stiffness matrix written according to the constitutive equations (4); $\mathscr{E}^{\circ}_m=\dfrac{1}{2A}\displaystyle\int_A\underline{\varepsilon}^{\mathrm{T}}\underline{\underline{C}}^m\underline{\varepsilon}\,da$ is the mean value of the micro-strain energy over the unit cell. According to the multi-scale kinematics here considered the micro-strain field $\underline{\varepsilon}=\{\varepsilon_{11}\quad\varepsilon_{22}\quad 2\varepsilon_{12}\}^{\mathrm{T}}$ in the heterogeneous cell may be written in the following linear form $\underline{\varepsilon}=\underline{\underline{B}}^E(\mathbf{z})\underline{E}+\underline{\underline{B}}^{\kappa}(\mathbf{z})\underline{\kappa}$, $\underline{\underline{B}}^E(\mathbf{z})$ and $\underline{\underline{B}}^{\kappa}(\mathbf{z})$ being matrices de-

pending on the functions $\theta^1_{ikl}(\mathbf{z})$ and $\theta^2_{iklp}(\mathbf{z})$, i.e. on the microstructure of the unit cell. As a consequence the mean value of the micro-strain energy turns out to be a quadratic form in the variables $\underline{E}$, $\underline{\kappa}$ and may be compared with the macro-strain energy (14) in order to obtain the sub-matrices

$$\underline{\underline{C}} = \frac{1}{A}\int_A \underline{\underline{B}}^{ET}\underline{\underline{C}}^m\underline{\underline{B}}^E \mathrm{d}a, \quad \underline{\underline{Y}} = \frac{1}{A}\int_A \underline{\underline{B}}^{ET}\underline{\underline{C}}^m\underline{\underline{B}}^\kappa \mathrm{d}a, \quad \underline{\underline{S}} = \frac{1}{A}\int_A \underline{\underline{B}}^{\kappa T}\underline{\underline{C}}^m\underline{\underline{B}}^\kappa \mathrm{d}a\,. \tag{15}$$

The matrices $\underline{\underline{C}}$ and $\underline{\underline{S}}$ are symmetric and because of the symmetry of the second-gradient strain $\kappa_{ijk} = \kappa_{ikj}$ the additional symmetries are obtained: $S_{i5} = S_{i7}$, $S_{i6} = S_{i8}$, $Y_{i5} = Y_{i7}$ and $Y_{i6} = Y_{i8}$, $i = 1,...,8$. In general, the stiffness matrix of the second-order elastic plane model is characterised by 45 elasticities (matrix $\underline{\underline{C}}$ - 6 elasticities, matrix $\underline{\underline{S}}$ - 21 elasticities, matrix $\underline{\underline{Y}}$ - 18 elasticities). In the case of centro-symmetric unit cell one obtains $\underline{\underline{Y}} = \underline{\underline{0}}$ and the first order-strain and the second-order strain are uncoupled.

Finally, the constitutive equations are written in the matrix form $\underline{\Sigma} = \partial\mathscr{E}^\circ_M / \partial\underline{E} = \underline{\underline{C}}\,\underline{E} + \underline{\underline{Y}}\,\underline{\kappa}$, $\underline{\mu} = \partial\mathscr{E}^\circ_M / \partial\underline{\kappa} = \underline{\underline{Y}}^{\mathrm{T}}\underline{E} + \underline{\underline{S}}\,\underline{\kappa}$, being the stress vectors written in the form $\underline{\Sigma} = \{\Sigma_{11} \quad \Sigma_{22} \quad \Sigma_{12}\}^{\mathrm{T}}$ and $\underline{\mu} = \{\mu_{111} \quad \mu_{222} \quad \mu_{122} \quad \mu_{211} \quad \mu_{121} \quad \mu_{212} \quad \mu_{112} \quad \mu_{221}\}^{\mathrm{T}}$, respectively.

4 IN-PLANE DISPERSIVE WAVES IN PERIODIC MASONRY

The homogenization technique presented in the previous Section allows to analyse the in-plane wave propagation in a masonry wall. Let us consider the wave propagation along the orthotropy direction $\mathbf{e}_\beta$, with $\beta = 1,2$, represented at the macro-scale by the component of the displacement vector $U_\alpha(y_\beta, t)$ with $U_\gamma \equiv 0$ where $\alpha,\beta,\gamma = 1,2$ and $\alpha \neq \gamma$ (see figure 3). The equation of motion of a second-order continuum is specialized to the case of an orthotropic material that is equivalent to a heterogeneous periodic material characterized by centro-symmetric unit cells and from equation (6) is written in the form

$$C_{\beta\alpha\beta\alpha}U_{\alpha,\beta\beta} - S_{\alpha\beta\beta\alpha\beta\beta}U_{\alpha,\beta\beta\beta\beta} = \rho_M\left(\ddot{U}_\alpha - J_{\beta\beta}\ddot{U}_{\alpha,\beta\beta}\right). \tag{16}$$

By noting that $\hat{c}^\alpha_\beta = \sqrt{C_{\beta\alpha\beta\alpha}/\rho_M}$ denotes the velocity of the longitudinal $(\alpha = \beta)$ and transverse $(\alpha \neq \beta)$ waves along direction $\mathbf{e}_\beta$ in a corresponding Cauchy continuum ($S_{\alpha\beta\beta\alpha\beta\beta} = J_{\beta\beta} = 0$ in equation (16)), $\lambda^\alpha_\beta = \sqrt{S_{\alpha\beta\beta\alpha\beta\beta}/C_{\beta\alpha\beta\alpha}}$ denotes the extensional $(\alpha = \beta)$ and shearing $(\alpha \neq \beta)$ characteristic length of the masonry bond as shown in [15], and $J_{\beta\beta} = \eta d^2$, being d the cell size and η a parameter that depends on the geometrical and mechanical properties of the cell, the displacement equation of motion may be written in the form

$$\left(\lambda^\alpha_\beta\hat{c}^\alpha_\beta\right)^2 U_{\alpha,\beta\beta\beta\beta} - \hat{c}^{\alpha 2}_\beta U_{\alpha,\beta\beta} = \ddot{U}_\alpha - \eta d^2\ddot{U}_{\alpha,\beta\beta}\,. \tag{17}$$

To evaluate the dispersion functions, the solution of equation (17) is considered having the form $U_\alpha(y_\beta, t) = A\exp\left[i\left(ky_\beta - \omega t\right)\right]$, where $i^2 = -1$, k is the wave number and ω is the an-

gular frequency. The wavelength and the phase velocity of the in-plane waves along direction $\mathbf{e}_\beta$ are $\lambda = 2\pi/k$ and $c_\beta^\alpha = \omega/k$, respectively. The dispersion function corresponding to the longitudinal $(\alpha = \beta)$ transverse $(\alpha \neq \beta)$ oscillatory motion of the derived equivalent continuum takes the following form

$$\omega = k\hat{c}_\beta^\alpha \sqrt{\frac{1+\lambda_\beta^{\alpha 2} k^2}{1+\eta d^2 k^2}} = k\hat{c}_\beta^\alpha \sqrt{\frac{1+4\pi^2\left(\lambda_\beta^\alpha/\lambda\right)^2}{1+4\pi^2\eta\left(d/\lambda\right)^2}}, \tag{18}$$

that depends on the wave number k. From equation (18) it results that for large wavelengths $(\lambda \to \infty)$ the angular frequency tends to the value related to the standard continuum, i.e $\omega \to k\hat{c}_\beta^\alpha$.

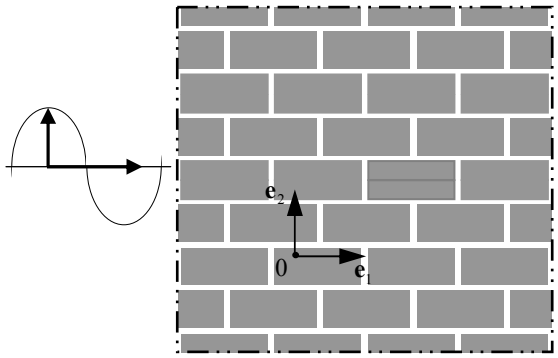

Fig. 3 Shear wave propagation along the orthotropy direction $\mathbf{e}_1$.

5 NUMERICAL EXAMPLES

The computational homogenization procedure described in the previous Sections has been applied to the in-plane analysis of both running bond and English bond masonry. In both cases the bricks and the mortar are assumed elastic and isotropic in order to assess the reliability of the procedure and to analyze the propagation of elastic waves. The two steps of the homogenization procedure are carried out by a FE analysis of the unit cell and the overall elastic moduli of the second-order equivalent continuum model are obtained for different stiffness ratios E_b/E_m, being E_b and E_m the Young's modulus of the brick and the mortar, respectively. Moreover, the unit cells analysed for the two considered masonry patterns are characterized by orthogonal axes of symmetry z_1 and z_2, so that the constitutive equations of the equivalent second-order continuum are orthotropic. The propagation of shear waves along the two axes of orthotropy z_1 and z_2 of the considered masonry bonds is analysed assuming the ratio $E_b/E_m = 10$ between the brick and the mortar Young modulus, respectively.

5.1 Running bond masonry

The considered running bond masonry having the unit square cell shown in figure 1.b is analysed. The brick dimensions are 120mm x 60mm and the mortar thickness is 10mm; the unit cell size is $d = 130$mm. The constituents are assumed isotropic, perfectly bonded and in plane stress condition. The Young's modulus $E_m = 500$MPa of the mortar is assumed and for

both the constituents equal Poisson ratios are assumed $\nu_m = \nu_b = 0.1$. The elastic moduli of the homogeneous equivalent continuum have been evaluated for increasing values of the Young modulus of the bricks ($E_b = 10 \div 10^3 E_m$) in order to appreciate the effect of mismatch in the elastic moduli of the constituents. The mass density for bricks and mortar are $\rho_b = 1600$ kg/m^3 and $\rho_m = 1500$ kg/m^3 respectively. The mass density at the macro-scale ρ_M and the inertia tensor components J_{11}, J_{22} take the following values: $\rho_M = 1585$ kg/m^3, $J_{11} = 1406$ mm^2, $J_{22} = 1410$ mm^2. The elastic moduli $\mathbb{C}$ obtained by the standard first-order (Cauchy) homogenization (first step of the homogenization) are given in Table 1. The elastic moduli $\mathbb{S}$, obtained in the second step of the homogenization for the second order continuum are given in Table 2.

Tab.1 Elastic moduli - first order (Cauchy) homogenization C_{ijhk} (MPa).

E_b	C_{1111}	C_{2222}	C_{1122}	C_{1212}
$10E_m$	2.763E+03	2.013E+03	1.794E+02	8.186E+02
$10^2 E_m$	6.194E+03	2.997E+03	1.587E+02	1.169E+03
$10^3 E_m$	7.136E+03	3.155E+03	1.287E+02	1.227E+03

Tab.2 Elastic moduli - second order homogenization S_{ijhkpq} (N).

E_b	S_{111111}	S_{222222}	S_{122122}	S_{211211}	S_{121121}	S_{212212}
$10E_m$	3.326E+04	1.912E+02	9.304E+04	3.778E+05	1.089E+06	5.682E+05
$10^2 E_m$	8.978E+04	6.827E+01	2.662E+05	1.959E+06	2.495E+06	7.483E+05
$10^3 E_m$	1.127E+05	1.077E+01	3.139E+05	2.687E+06	2.942E+06	7.847E+05

E_b	S_{111122}	S_{111212}	S_{222211}	S_{222121}	S_{122212}	S_{211121}
$10E_m$	2.707E+04	1.669E+04	-5.686E+01	9.817E+01	-9.506E+04	1.922E+05
$10^2 E_m$	5.992E+04	3.478E+04	-4.069E+02	-1.401E+02	-2.165E+05	6.907E+05
$10^3 E_m$	5.720E+04	4.707E+04	-1.249E+02	6.976E+01	-2.377E+05	8.376E+05

The characteristic lengths associated to the shear and to extensional strain along directions z_1 and z_2 take the form

$$\lambda_{Sh-1} = \lambda_1^2 = \sqrt{\frac{S_{211211}}{C_{1212}}}, \quad \lambda_{Sh-2} = \lambda_2^1 = \sqrt{\frac{S_{122122}}{C_{1212}}},$$
$$\lambda_{Ext-1} = \lambda_1^1 = \sqrt{\frac{S_{111111}}{C_{1111}}}, \quad \lambda_{Ext-2} = \lambda_2^2 = \sqrt{\frac{S_{222222}}{C_{2222}}}, \tag{19}$$

respectively, and the numerical values for the considered unit cell are given in Table 3. In Table 3 it is observed that when decreasing the stiffness mismatch between the brick and mortar E_b/E_m , the characteristic lengths associated with one-dimensional shear and extensional problems tend to zero.

Tab.3 Characteristic lengths (mm) of the homogeneous second-order model.

E_b	λ_{Sh-1}	λ_{Sh-2}	λ_{Ext-1}	λ_{Ext-2}
$10E_m$	21.5	10.7	3.5	0.31
$10^2 E_m$	40.9	15.1	3.8	0.15
$10^3 E_m$	46.8	16.0	4.0	0.06

The shear dispersive waves along directions $\mathbf{e}_\beta$, $\beta = 1,2$, for $E_b/E_m = 10$ are described in terms of the dispersion functions. The diagrams representing the dimensionless dispersion $\omega d/\hat{c}_1^2$ as a function of the dimensionless wavenumber kd are shown in figure 4 (red line $\mathbf{e}_1$ propagation, blue line $\mathbf{e}_2$ propagation) and compared with the corresponding one referred to the first-order continuum (black straight line). The group velocity $c_{g-\beta}^{\alpha}/\hat{c}_1^2$ and the phase velocity $c_\beta^\alpha/\hat{c}_1^2$ as functions of the wavelength are shown in figure 5, respectively. Unlike the first order continuum (Cauchy), where the frequency is proportional to the wave number, dispersive waves propagate in the second-order equivalent continuum with phase velocity c_β^α and group velocity $c_{g-\beta}^{\alpha} = \dfrac{\mathrm{d}\omega}{\mathrm{d}k}$ which differ at different wave numbers. In the Running bond pattern an appreciable difference between the results provided by the equivalent second-order continuum and the corresponding ones by the standard Cauchy continuum are observed in the diagrams of figures 4 and 5. For wavelength $\lambda = 5d$ from the diagrams in figure 5 one obtains $c_{g-1}^2 \approx 0.85\hat{c}_1^2$ and $c_1^2 \approx 0.94\hat{c}_1^2$.

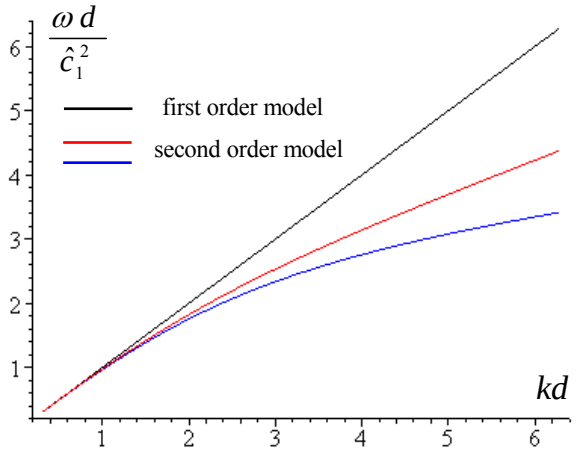

Fig. 4 Dimensionless dispersion functions. Red line $\mathbf{e}_1$ propagation, blue line $\mathbf{e}_2$ propagation; black line: first-order continuum.

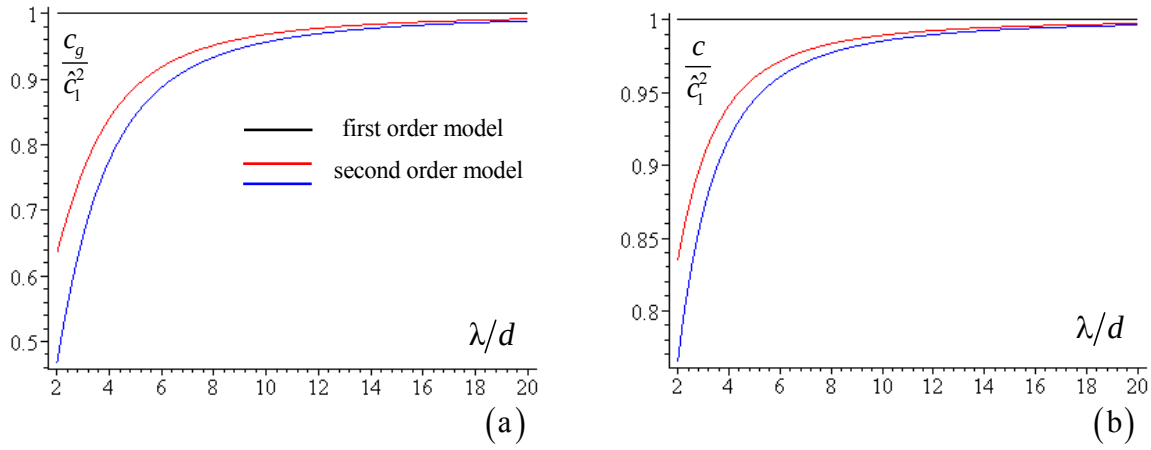

Fig. 5 Group and phase velocities. Red line $\mathbf{e}_1$ propagation, blue line $\mathbf{e}_2$ propagation; black line: first-order continuum.

5.2 English bond masonry

The English bond masonry having the rectangular unit cell shown in figure 6, with sides $d_1 = 260\text{mm}$, $d_2 = 140\text{mm}$, is considered. The brick dimensions are 250mm x 120mm x 60mm and the mortar thickness is 10mm. The constituents are assumed isotropic, perfectly bonded and in plane stress condition; the Young modulus $E_m = 500\text{MPa}$ is assumed for the mortar and equal Poisson ratio is assumed $\nu_m = \nu_b = 0.1$ for both the constituents. The elastic moduli of the homogeneous equivalent continuum have been evaluated for increasing values of the Young modulus of the bricks ($E_b = 10 \div 10^3 E_m$). The mass density for bricks and mortar are $\rho_b = 1600\ \text{kg/m}^3$ and $\rho_m = 1500\ \text{kg/m}^3$ respectively. The mass density at the macro-scale ρ_M and the inertia tensor components J_{11}, J_{22} take the following values: $\rho_M = 1581\ \text{kg/m}^3$, $J_{11} = 5625\ \text{mm}^2$, $J_{22} = 1638\ \text{mm}^2$. The elastic moduli $\mathbb{C}$ obtained by the standard first-order (Cauchy) homogenization (first step of the homogenization) are given in Table 4. The elastic moduli $\mathbb{S}$, obtained in the second step of the homogenization for the second order continuum are given in Table 5. Moreover, the characteristic lengths associated to the shear and to extensional strain along directions z_1 and z_2 (see relation (19)) for the considered unit cell are given in Table 6.

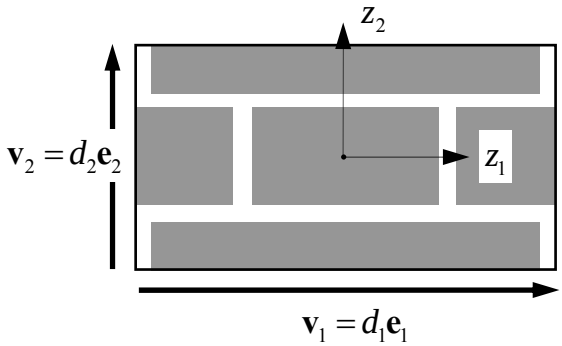

Fig. 6 Unit cell for English bond patterns.

Tab.4 Elastic moduli first order (Cauchy) homogenization C_{ijhk} $\left(\mathrm{MPa}\right)$.

E_b	C_{1111}	C_{2222}	C_{1122}	C_{1212}
$10E_m$	3.101E+03	2.125E+03	1.911E+02	8.756E+02
$10^2 E_m$	8.799E+03	3.239E+03	1.757E+02	1.279E+03
$10^3 E_m$	1.112E+04	3.422E+03	1.345E+02	1.346E+03

Tab.5 Elastic moduli second order homogenization S_{ijhkpq} $\left(\mathrm{N}\right)$.

E_b	S_{111111}	S_{222222}	S_{122122}	S_{211211}	S_{121121}	S_{212212}
$10E_m$	1.022E+05	1.905E+02	7.147E+04	8.394E+05	1.641E+06	2.647E+06
$10^2 E_m$	5.177E+05	3.001E+02	2.041E+05	4.486E+06	5.373E+06	3.821E+06
$10^3 E_m$	7.782E+05	4.287E+01	2.436E+05	6.179E+06	7.385E+06	3.999E+06

E_b	S_{111122}	S_{111212}	S_{222211}	S_{222121}	S_{122212}	S_{211121}
$10E_m$	3.760E+04	2.795E+04	-1.831E+01	-1.216E+02	-2.495E+05	4.454E+05
$10^2 E_m$	1.083E+05	7.246E+04	-4.107E+03	-1.832E+03	-6.113E+05	1.947E+06
$10^3 E_m$	1.096E+05	1.125E+05	-1.497E+03	1.977E+01	-7.059E+05	2.396E+06

Tab.6 Characteristic lengths $\left(\mathrm{mm}\right)$ of the homogeneous second-order model.

E_b	λ_{Sh-1}	λ_{Sh-2}	λ_{Ext-1}	λ_{Ext-2}
$10E_m$	31.0	9.0	5.7	0.30
$10^2 E_m$	59.2	12.6	7.7	0.30
$10^3 E_m$	67.7	13.5	8.4	0.11

The diagrams representing the dimensionless dispersion $\omega d_2/\hat{c}_1^2$ as a function of the dimensionless wavenumber kd_2 are shown in figure 7 for $E_b/E_m = 10$; the group velocity $c_{g-\beta}^{\alpha}/\hat{c}_1^2$ and the phase velocity $c_{\beta}^{\alpha}/\hat{c}_1^2$ as functions of the wavelength are shown in the diagrams of figure 8. From these diagrams a remarkable difference between the results provided by equivalent second-order continuum and the corresponding ones from the standard Cauchy continuum are observed. For wavelength $\lambda = 5d_2$ one obtains $c_{g-1}^2 \approx 0.65\hat{c}_1^2$ and $c_1^2 \approx 0.85\hat{c}_1^2$.

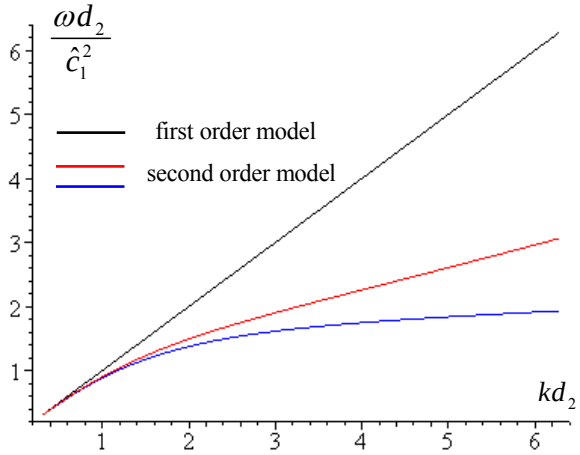

Fig. 7 Dimensionless dispersion functions. Red line $\mathbf{e}_1$ propagation, blue line $\mathbf{e}_2$ propagation; black line: first-order continuum.

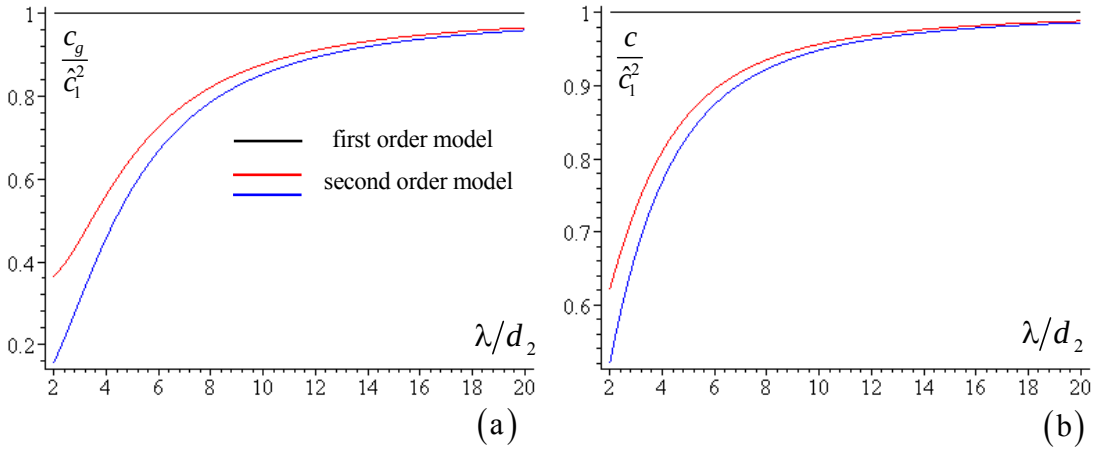

Fig. 8 Group and phase velocities. Red line $\mathbf{e}_1$ propagation, blue line $\mathbf{e}_2$ propagation; black line: first-order continuum.

6 CONCLUSIONS

The in-plane static and dynamic response of elastic periodic masonry is analyzed on the basis of a second order homogenization technique that is developed by considering an enhanced representation of the micro-displacement field at the brick scale in terms of the macro-kinematics at the structural scale. This kinematical micro-macro framework guarantees the continuity of the micro-displacement field in the representative unit cell and across the interfaces between adjacent unit cells. A computationally efficient procedure is developed which is applied in two steps: the first step corresponds to the standard homogenization, while the second step, that is based on the results of the first step, completes the second-order homogenization. Moreover, it is shown that in the equivalent second-order model dispersive waves propagate.

Running bond and English bond masonry are analysed in the examples to illustrate the capabilities of the homogenization techniques. The overall elastic moduli and the characteristic lengths of the second-order equivalent continuum are obtained by the computational homogenization carried out by the FE analysis of the unit cell and the effects of the stiffness mismatch between the brick phase and the mortar phase are considered.

Finally, it is shown that for wavelengths shorter than ten times the average brick unit size the propagation of elastic waves in the second-order homogenized model takes place with appreciable differences in the phase and group velocities with respect to the standard Cauchy model.

7 ACKNOWLEDGMENT

The authors acknowledge financial support of the (MURST) Italian Department for University and Scientific and Technological Research in the framework of the research MIUR Prin07 project 2007YZ3B24, *Multi-scale problems with complex interactions in Structural Engineering*, coordinated by prof. A. Corigliano.

REFERENCES

[1] R. Masiani, N. Rizzi, P. Trovalusci, Masonry as structured continuum, *Meccanica*, **30**, 673-683, 1995.

[2] J. Sulem, H.B. Mühlhaus, A continuum model for periodic two-dimensional block structures, *Mech. Cohesive-frictional Materials*, **2**, 31-46, 1997.

[3] G. Salerno, G. de Felice, Continuum modeling of periodic brickwork, *Int. J. Solids and Structures*, **46** ,1251-1267, 2009.

[4] Stefanou I., Sulem J., Vardoulakis I., Three-dimensional Cosserat homogenization of masonry structures: elasticity, *Acta Geotecnica*, **3**, (1), 71-83, 2008.

[5] S. Casolo, Macroscopic modelling of structured materials: Relationship between orthotropic Cosserat continuum and rigid elements, *Int. J. Solids and Structures*, **43** ,475-496, 2006.

[6] S. Forest, K. Sab, Cosserat overall modeling of heterogeneous materials, *Mechanics Research Communications*, **25**, 449-454, 1998.

[7] Bacigalupo A., Gambarotta L., Cosserat homogenization of elastic periodic blocky masonry, *8th World Congress on Computational Mechanics* (Venice), Schrefler B. Perego U. Eds., 2 pagg, ISBN 9788496736559, CIMNE, 2008.

[8] A. Bacigalupo, L. Gambarotta, Non-Local Computational Homogenization of Periodic Masonry, *Int. J. for Multiscale Computational Engineering*, to appear, 2011.

[9] D. Addessi, E. Sacco, A. Paolone, Cosserat model for periodic masonry deduced by nonlinear homogenization, *European Journal of Mechanics A/Solids*, **29**, 724-737, 2010.

[10] N.S. Bakhvalov, G.P. Panasenko, *Homogenization: Averaging Processes in Periodic Media*. Nauka, Moscow (in Russian). English translation in: Mathematics and its Applications (Soviet Series) 36, Kluwer Academic Publishers, Dordrecht-Boston-London, 1984.

[11] C. Boutin, Microstructural effects in elastic composites, *Int. J. Solids and Structures*, **33** ,1023-1051, 1996.

[12] N. Triantafyllidis, S. Bardenhagen, The influence od scale size on the stability of periodic solids and the role of associated higher order gradient continuum models, *J. Mechanics and Physics of Solids*, **11**, 1891-1928, 1996.

[13] V.P. Smyshlyaev, K.D. Cherednichenko, On rigorous derivation of strain gradient effects in the overall behaviour of periodic heterogeneous media, *J. Mechanics and Physics of Solids*, **48**, 1325-1357, 2000.

[14] R.H.J. Peerlings, Fleck N.A., Computational Evaluation of Strain Gradient Elasticity Constants, Int. J. for Multiscale Computational Engineering, 2, 599-619, 2004.

[15] A. Bacigalupo, L. Gambarotta, Second-order computational homogenization of heterogeneous materials with periodic microstructure, *ZAMM Z. Angew. Math. Mech.*, **90**, No. 10–11, 796 – 811, 2010.

[16] R.D. Mindlin, Micro-structure in linear elasticity, *Arch. Ration. Mech. Anal.*, **16**, 51–78, 1965.

[17] P. Germain, The method of virtual power in continuum mechanics. Part 2: microstructure, *SIAM J. Appl. Math.* , **25** (3), 556–575, 1973.